CrossMark

RESEARCH

First principle study of the effect of defects on performance of single-molecule pentacene field effect transistors

Bahniman Ghosh[1,2] · Akash Gramin[2]

Abstract In this work, we have performed first principle study on a single-molecule pentacene field effect transistor and studied various oxygen- and hydrogen-induced defects in the same device configuration. Further, we have investigated the effect of these defects on the various electronic transport properties of the device and compared them with those of the original device along with reporting the negative differential region window and the peak-to-valley ratio in different cases. For this purpose, we have applied the density functional theory in conjugation with non-equilibrium green's function (NEGF) formalism on a 14.11 Å pentacene device to obtain the I–V characteristics, conductance curves and transmission spectra in various device scenarios.

Introduction

In the recent times, organic semiconductors have generated significant interest in the research and academic community. Due to the extensive application, possibilities of these materials in various areas such as organic flexible displays, smart devices and cards, solar cells and light-emitting diodes (OLED) among many others as well as the advantage of having low-cost, simpler processing and manufacturing techniques have led to an immense pace of development of these materials [1–5]. Moreover, consistent and rapid improvements in both device function and efficiency of organic-based devices have been promising in realizing "completely organic" (i.e., inorganic less) solutions [6]. So much so, that it would not be surprising to see organic-based mainstream commercial products in the coming few years. With this, organic electronics is already dubbed as being the next big revolution in the field of microelectronics.

Out of these, aromatic hydrocarbons have gained much attention with regard to their application in molecular devices [7]. Pentacene has been one of the most encouraging materials in realizing organic transistor, as it offers better reliability, mobility, stability and on–off ratio than many other organic materials [8]. Pentacene ($C_{22}H_{14}$) is an aromatic organic molecule with planar geometry having five benzene rings fused alongside each other as shown in Fig. 1a. It generally occurs in a herringbone pattern to form a triclinic structure having two molecules in a single unit cell. There are many different types of pentacene polytypes [9–11]. The electronic and structural properties of pentacene have been studied in some detail for single molecule and molecular solid systems [12]. In [13], authors study the physics of electron transport in single molecule. In [14], authors perform theoretical investigations of transport behavior in single molecule covalently bonded to gold electrodes. Although the effects of defects and impurities on mobility in pentacene crystal have been studied earlier in some detail, there has not been any study on pentacene single molecule field effect transistor (FET) [15].

In this work, we have applied non-equilibrium green's function (NEGF) formalism in conjugation with density

✉ Bahniman Ghosh
bghosh@utexas.edu

[1] Microelectronics Research Center, University of Texas at Austin, 10100 Burnet Road, Bldg. 160, Austin, TX 78758, USA

[2] Department of Electrical Engineering, Indian Institute of Technology Kanpur, Kanpur 208016, India

 Springer
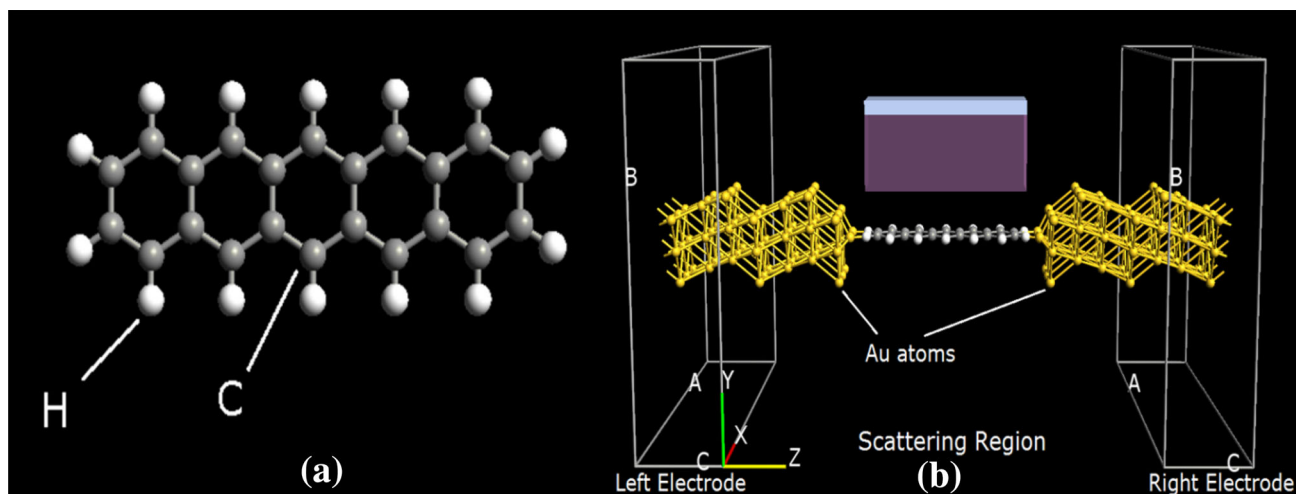
Fig. 1 a An isolated pentacene ($C_{22}H_{14}$) molecule. **b** Single-molecule pentacene FET with a pentacene molecule between the two gold electrodes

functional theory (DFT) to carry out first principle studies of the effect of oxygen- and hydrogen-induced defects on the electronic transport properties of a single pentacene molecule-based FET. We have also investigated additional properties in the I–V characteristics such as negative differential resistance (NDR) behavior, which is defined as the region on the I–V curve where an increase in the applied potential results in a decrease in the corresponding current (negative slope) and peak-to-valley ratio (PVR), which is the ratio of maximum peak current to the minimum valley current through the device, under different device scenarios.
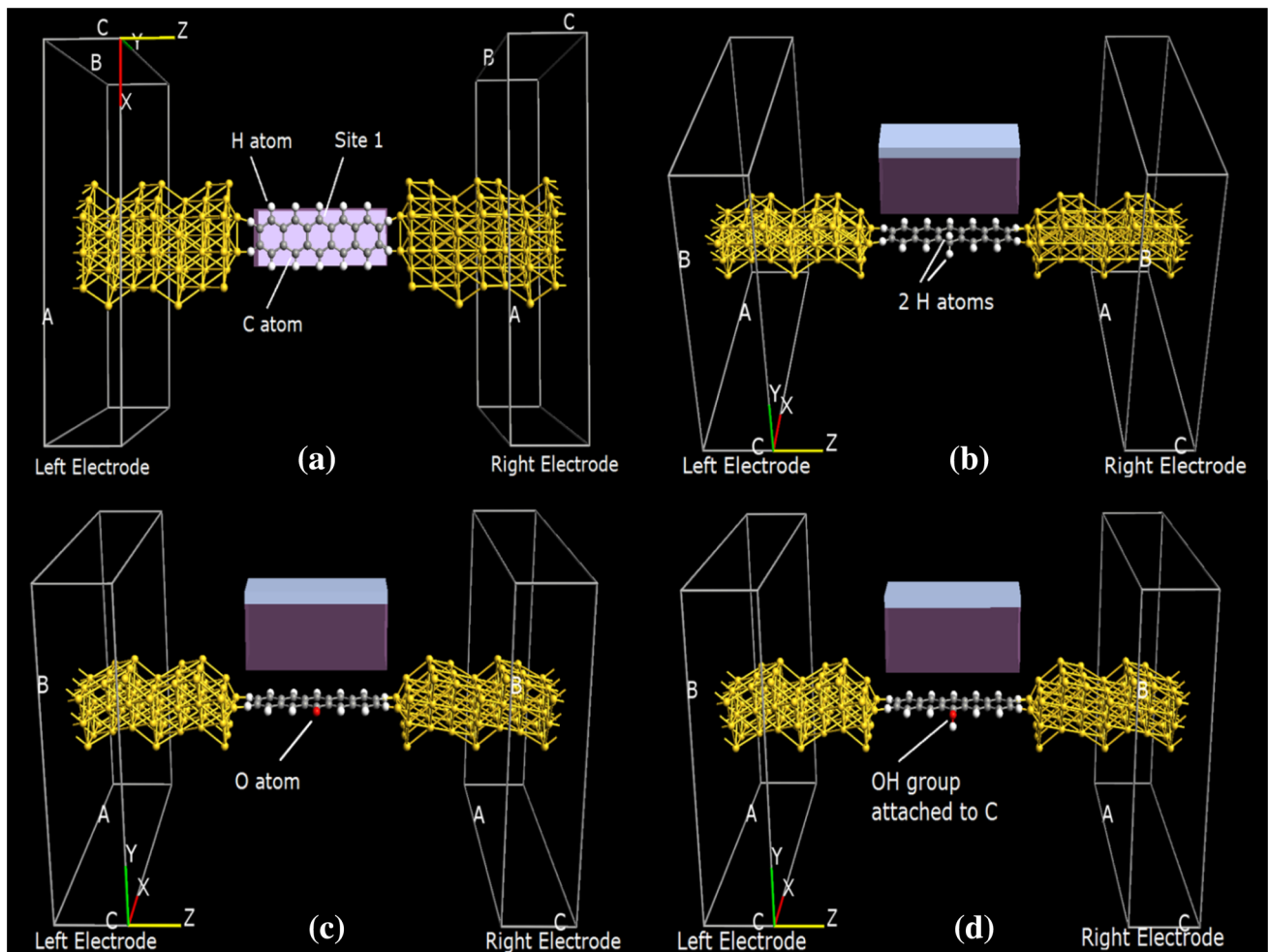
Model

In our model, we have sandwiched a pentacene molecule between two gold electrodes thus making a FET configuration as shown in Fig. 1b. The nature of chemical bonding of a pentacene to gold is a van der Waals type. We find a supercell that can hold pentacene crystal on the Au(111) surface. A very good match with a mean strain below 2 percent is obtained through repetition of the Au(111) into a $(2 \times 3\sqrt{3})$ structure. For pentacene on the Au(111) surface, we obtained work function difference of 0.97 eV. The difference in work function arises from the charge transfer from gold to pentacene which gives rise to an interface dipole. This shows up in the electrostatic difference potential. The gate voltage (V_g) is applied only on top of the pentacene molecule. The entire device has three parts: the right electrode (R), central scattering region (SR) and left electrode (L). The gold electrodes are extracted along (111) direction from bulk gold, [16–18]. The pentacene molecule is attached to the two electrodes

on either side. The bond lengths between the molecule and the electrodes along with the overall geometry of the configuration are determined by total energy optimizations in which the distance between electrodes is fixed. In this manner, the configuration is completely optimized such that the maximum atomic force between the atoms in less than 0.05 eV/Å, without disturbing the electrode gold atoms. Device channel length is 14.11 Å and width is 4.93 Å. The size of the supercell in the y-direction is taken as 26.66 Å. Also, HfO_2 ($\varepsilon_r = 25$) is used as the gate dielectric material with oxide thickness equal to 5.5 Å.

We have studied three types of defects in the pentacene ($C_{22}H_{14}$) molecule device which are namely, $C–H_2$ defect, C–O defect and C–HOH defect. The $C–H_2$ defect is created by adding one H atom to any one of the C–H units thus making it $C–H_2$ unit and the $C_{22}H_{14}$ molecule, a $C_{22}H_{15}$ one. Although the H atom can be connected to any of the corner C atoms, the most stable configuration is formed when it is attached as shown in Fig. 2a [19]. Similarly, the C–O defect is created by replacing an H atom with an O atom thus forming a double bond with that C atom and making it fourfold coordinated. In the same fashion, the C–HOH defect is formed by adding an OH group to the same C as mentioned above and further shown in the Fig. 2d. All the three defect configurations are optimized for geometry and bond relaxation. Next after the geometrical optimizations, all the three configurations are studied for electronic transport properties.

For all the electronic transport and geometry optimization study-related calculations of the configuration, we have used Atomistix ToolKit (ATK) simulator which is based on the combined theories of NEGF and DFT (NEGF + DFT) [20–22]. The exchange–correlation

Fig. 2 **a** *Bottom view* of the device showing the C atom (site 1) where the most stable defects are formed. **b** device with C–H$_2$ defect. (C$_{22}$H$_{15}$) **c** device with C–O defect (C$_{22}$H$_{13}$O) **d** device with C–HOH defect (C$_{22}$H$_{15}$O)

potential in our model is described by the Perdew–Zunger functional of the local density approximation (LDA.PZ). The basis set used is a double zeta polarized (DZP) basis for all the atoms. First principle norm-conserving Fritz-Haber-Institute (FHI) pseudo-potentials are employed and the energy correlation functional is spin independent [23]. The electrode Poisson solver calculations are carried out with boundary conditions as periodic and the Brillouin zone integration is carried out with $1 \times 10 \times 100$ k-point sampling. A real space grid is used for computing electrostatic potentials, with mesh cutoff energy equal to 75 Hartree. The electron temperature is taken as 300 K. Moreover, a large supercell dimension is taken in the perpendicular direction of electronic transport so that there is minimal or no interaction among the pentacene molecule and its images. As per the NEGF formalism, the current I_{s-d} flowing between the source and drain terminals of the device resulting from applying a source–drain bias V_{s-d} is given by the following formula [22]:

$$I_{s-d} = \frac{2e}{h} \int T(E, V_{s-d})[f(E - \mu_L) - f(E - \mu_R)]dE,$$

$$(1)$$

where e and h are electron charge and Planck's constant, respectively, $\mu_{L(R)} = E_F \pm eV/2$ represents the electrochemical potential of the two electrodes and E_F denotes the Fermi level of the configuration which is taken to be zero. The electron Fermi distribution function of the electrodes is represented by $f(E - \mu_{L(R)})$. The total transmission probability is denoted by $T(E, V_{s-d})$ at energy E and source–drain bias V_{s-d}, and can be evaluated using:

$$T(E, V_{s-d}) = \text{Tr}[\Gamma_L G^R \Gamma_R G^A],$$

$$(2)$$

where $G^{R(A)}$ denotes the retarded (advanced) Green's function, and $\Gamma_{L(R)} = i\left[\sum_{L(R)}^{R} - \sum_{L(R)}^{A}\right]$ denotes the contact broadening function with $\sum_{L(R)}^{R}$ and $\sum_{L(R)}^{A}$ being the self-energy

terms containing the effect of the electrodes. By shifting the SR terms of the Hamiltonian along with V_g, the effect of gate voltage is accounted for. Further details on such a theoretical arrangement can be studied in Refs. [20, 22].

Results and discussions

In all the cases, the applied gate voltage is taken 0.4 V while the drain voltage is taken over a range of 0–0.8 V.

In Fig. 3a, the I–V characteristic of the original pentacene device without any defect is shown. The device exhibits square-law-type characteristics, with saturated output curves, negative differential resistance regions and a low on-current. As can be clearly seen from the plot, the channel current shows a rising edge at zero bias voltage. The maximum current through the channel is of magnitude 2350 nA which is achieved at 0.42 V bias voltage. Also, the minimum channel current is observed at 0.74 V bias voltage and is equal to 1200 nA. Another important

(a) **(b)**
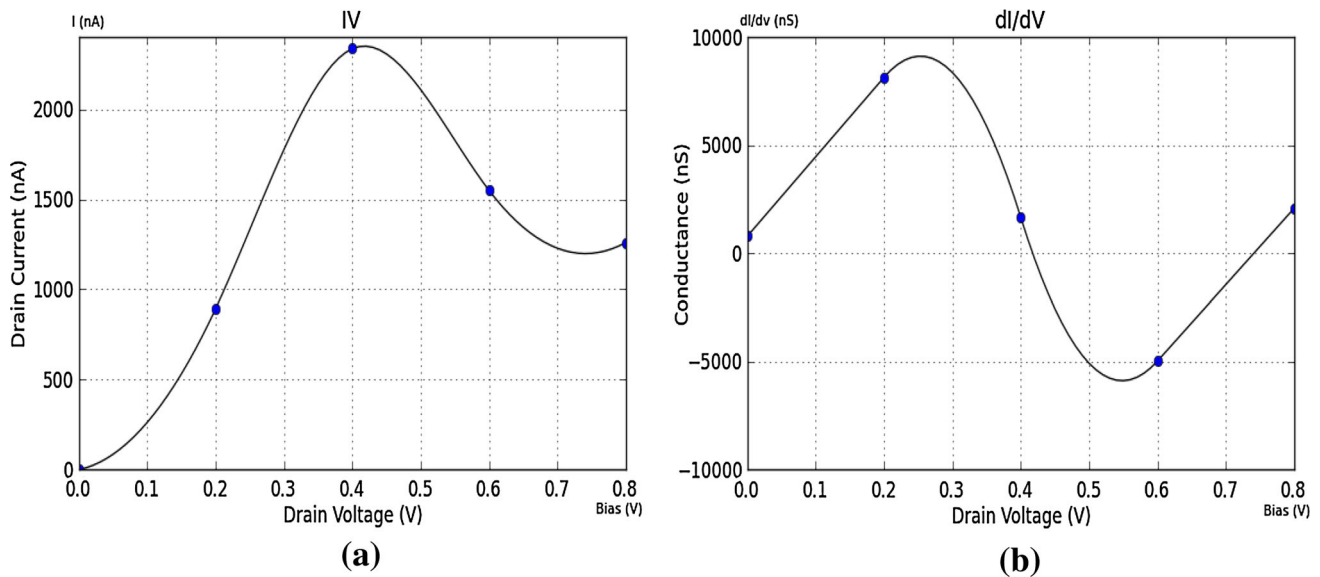
Fig. 3 **a** I–V characteristics of normal device ($V_g = 0.4$ V) **b** conductance of normal device ($V_g = 0.4$ V)

(a) **(b)**
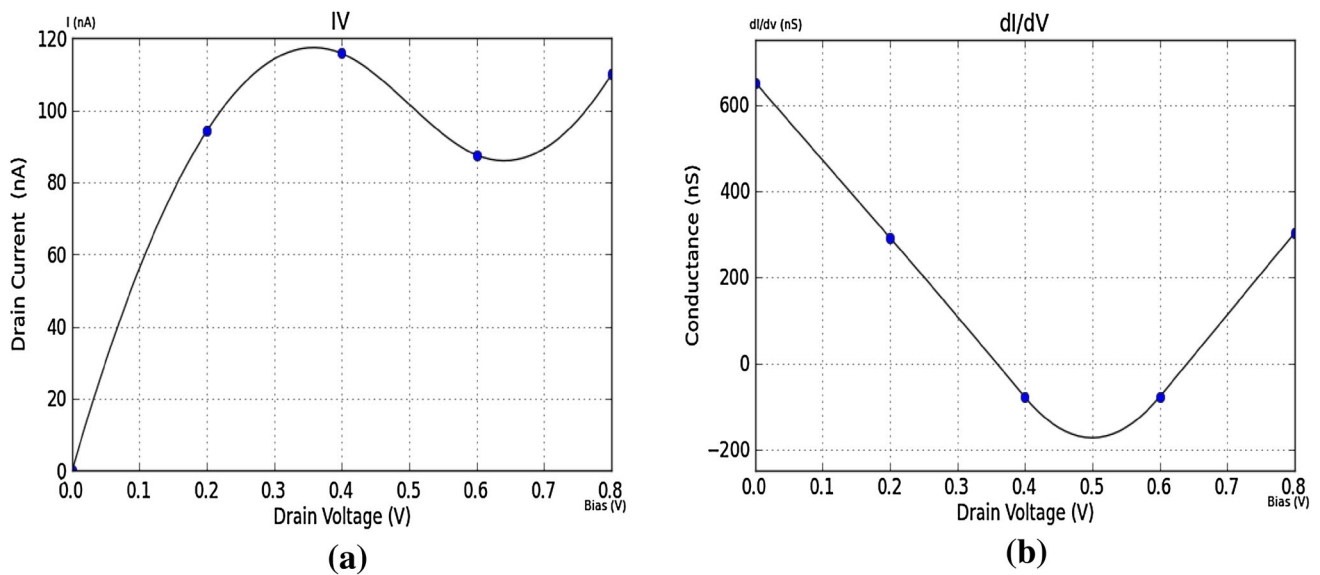
Fig. 4 **a** I–V characteristics of device with C–H$_2$ defect ($V_g = 0.4$ V). **b** Conductance of device with C–H$_2$ defect ($V_g = 0.4$ V)

observation is to note the NDR region which extends from 0.42 to 0.74 V drain voltage with PVR window of 1150 nA. The conductance vs bias voltage plot is shown in Fig. 3b, in which the peak conductance is seen at 0.25 V bias voltage which then decreases until it attains minima at 0.55 V bias voltage and increases afterwards.

Figure 4a shows the I–V curve of the device with C–H$_2$ defect. As can be seen from the plots, the channel current shows a rising edge at zero bias voltage. In this case, the maximum current is achieved at a bias voltage of 0.36 V, of magnitude 116 nA. The channel current then decreases with increasing bias voltage until achieving a minimum at 0.64 V bias voltage with corresponding channel current of 86 nA and increases afterwards. The NDR region is seen to extend from 0.36 to 0.64 V bias voltage and PVR windows of 30 nA. As the drain voltage is increased beyond 0.36 V, some of the transmission modes close to the Fermi level are suppressed. This leads to NDR behavior in I–V curves. Also, conductance decreases till it reaches 0.5 V at which point it starts to increase as shown in Fig. 4b.
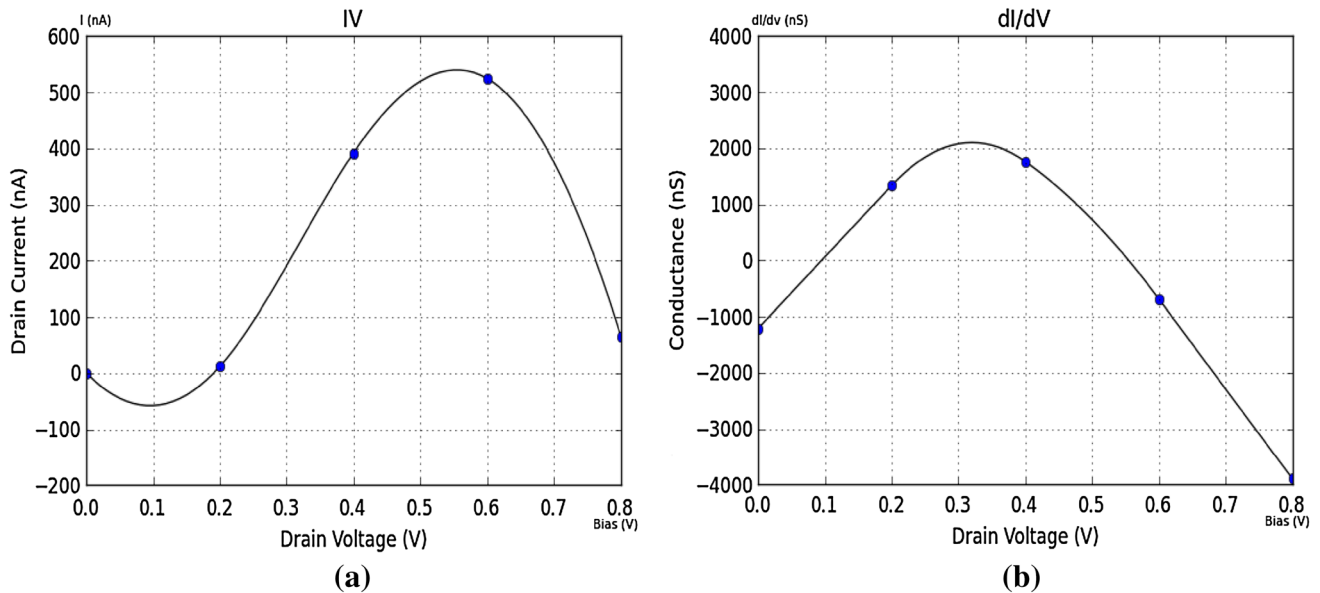

Fig. 5 **a** I–V characteristics of device with **b** conductance plot of the device with C–O defect ($V_g = 0.4$ V) C–O defect ($V_g = 0.4$ V)
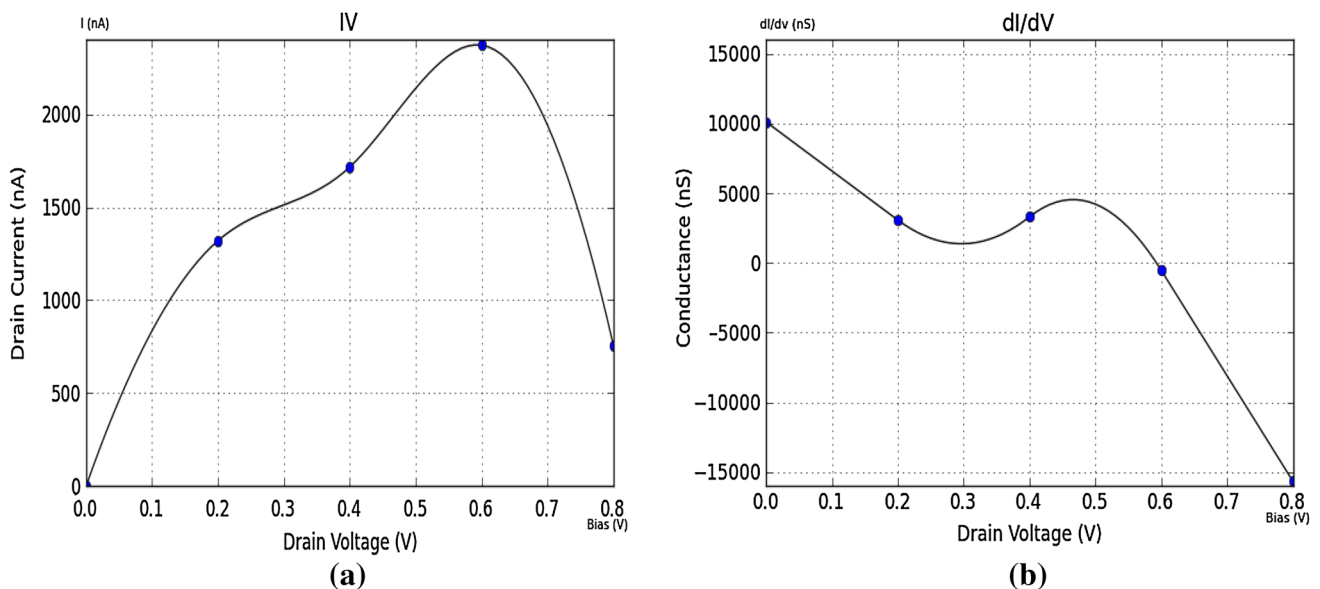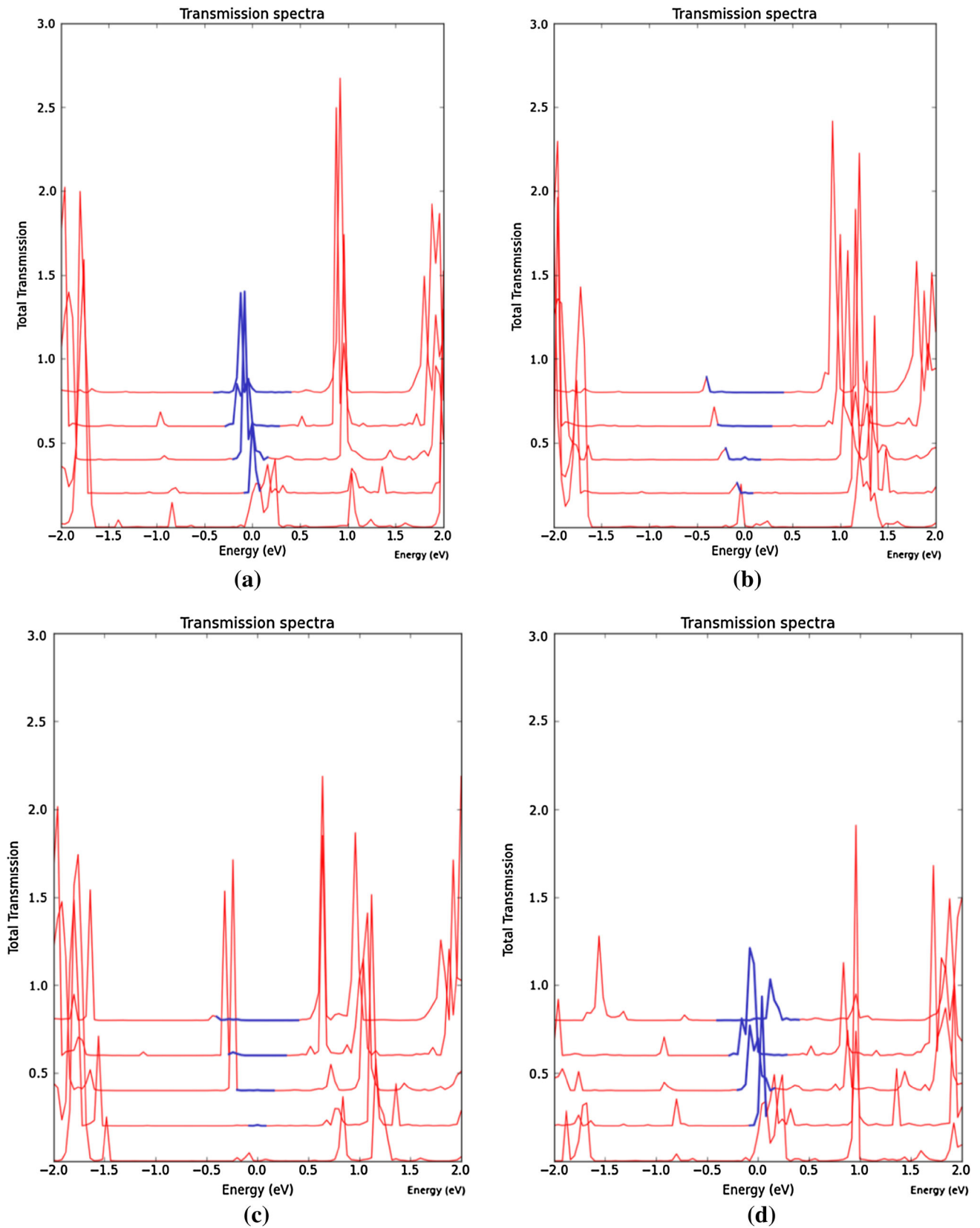

Fig. 6 **a** I–V characteristics of device with **b** conductance plot of the device with C–HOH defect ($V_g = 0.4$ V) C–HOH defect ($V_g = 0.4$ V)

Fig. 7 Transmission spectra corresponding to all the four cases: **a** normal device with no defect **b** device with C–H$_2$ defect **c** device with C–O defect **d** device with C–HOH defect

In Fig. 5a, the I–V characteristic of the device with C–O defect is shown. As the plot shows, the channel current shows a falling edge at zero bias voltage. In this case, the channel current first decreases till 0.1 V at which point its magnitude is 60 nA in the reverse direction and then increases till it reaches the bias voltage of 0.55 V where it attains a maximum of 530 nA and then decreases further on. The NDR region in this case can be seen to exist in two intervals, i.e., from 0 to 0.1 V and from 0.55 V onwards with PVR window of 590 nA. Figure 5b shows the conductance curve which attains a maximum of 2100 nA at bias voltage of 0.33 V.

In Fig. 6a, the I–V characteristic of the device with C–HOH defect is shown. As is evident from the plot, the curve shows a rising edge at zero bias voltage. In this case, the channel current increases till it achieves a maximum at 0.6 V bias voltage with corresponding current of 2475 nA after which it decreases further right being 550 nA at 0.8 V. The NDR region can be seen to start from this point (0.6 V) onwards with PVR window of 1925 nA. Also, Fig. 6b shows the conductance plot which decreases until it reaches 0.3 V where it attains minima and then increases slightly till 0.46 V and then decreases steadily. As the drain voltage is increased beyond 0.6 V, some of the transmission modes close to the Fermi level get suppressed and as explained earlier this results in drop in the transmission transparency of the channel, thus exhibiting NDR behavior.

The transmission spectra corresponding to all the four cases are shown in Fig. 7.

Conclusion

We have studied the effect of various hydrogen (H)- and oxygen (O)-induced defects, namely, C–H$_2$ defect, C–O defect and C–HOH defect on the I–V characteristics, conductance and transmission spectrum of single-molecule pentacene FET and compared them with the results of the device with no defects. We found that the channel current shows a significant decrease in the case of C–H$_2$ and C–O defect, while the results of C–HOH defect are comparable to those of the normal device with no defects. We have also reported the NDR region in all the four cases and learned that its range is comparable in the case of no defect and C–H$_2$ defect, while that of C–O defect is comparable to C–HOH defect along with reporting the PVR window. These properties of the single-molecule FET can be used in various applications such as in the development of SRAMs, high-frequency oscillators and sensors.

References

1. Sun, Y., Liu, Y., Zhu, D.: J. Mater. Chem. **15**, 53 (2005)
2. Murphy, A.R., Fréchet, J.M.J.: Chem. Rev. **107**, 1066 (2007)
3. Anthony, J.E.: AngewandteChemie Int. Ed. Engl **47**, 452 (2008)
4. Allard, S., Forster, M., Souharce, B., Thiem, H., Scherf, U.: AngewandteChemie Int. Ed. Engl. **47**, 4070 (2008)
5. Yamashita, Y.: Sci. Technol. Adv. Mater. **10**, 024313 (2009)
6. Koch, Norbert: Chem Phys Chem **8**, 1438–1455 (2007)
7. Horowitz, G.: Adv. Mater. **10**, 365 (1998)
8. Volkman, S.K., Molesa, S., Mattis, B., Chang, P.C., Subramanian V.: Mater. Res. Soc. Symp. Proc. 769, (2003)
9. Siegrist, T., et al.: AngewandteChemie Int. Ed. Engl. **40**, 1732 (2001)
10. Campbell, R.B., Robertson, J.M., Trotter, J.: Acta Crystallogr. **15**, 289 (1962)
11. Tiago, M.L., Northrup, J.E., Louie, S.G.: Phys Rev B **67**, 115212 (2003)
12. Endres, R.G., Fong, C.Y., Yang, L.H., Witte, G., Woll, C.: Materials Science (cond-mat.mtrl-sci)arXiv:cond-mat/0211420. (2002)
13. Chen, F., Tao, N.J.: Electron transport in single molecules: from benzene to graphene. Acc. Chem. Res. **42**, 429–438 (2009)
14. Li, X.L., Xu, B.Q., Xiao, X.Y., Hihath, J., Tao, N.J.: Measurement of electron transport Properties of single molecules. J. Jpn. Appl. Phys. **44**, 5344–5347 (2005)
15. Jurchescu, O.D., Baas, J., Palstra, T.T.M.: Appl. Phys. Lett. **84**, 3061 (2004)
16. Zheng, X.H., Shi, X.Q., Dai, Z.X., Zeng, Z.: Phys. Rev. B **74**, 085418 (2006)
17. Taylor, J., Brandbyge, M., Stokbro, K.: Phys. Rev. B **68**, 121101 (2003)
18. Ke, S.-H., Baranger, H.U., Yang, W.: Phys. Rev. B **71**, 113401 (2005)
19. Northrup, J.E., Chabinyc, M.L.: Phys. Rev. B **68**, 041202(R) (2003)
20. Taylor, J., Guo, H., Wang, J.: Physical Review B **63**, 245407 (2001)
21. Brandbyge, M., Mozos, J.L., Ordejón, P., Taylor, J., Stokbro, K.: Phys. Rev. B **65**, 165401 (2002)
22. Atomistix Virtual Nanolab, QuantumWise Inc
23. Troullier, N., Martins, J.: Phys. Rev. B **43**, 10222 (1991)
24. Buttiker, M., Landauer, R.: Phys. Rev. B **31**, 6207 (1985)